AO4ELT7 - June 2023 - Avignon

Performance of large-format deformable mirrors constructed with hybrid variable reluctance actuators III: laboratory measurements of dynamic behavior

Rachel Bowens-Rubin[a], Abraham Marsh[a], Philip Hinz[a], Caesar Laguna[a], Arjo Bos[b], Stefan Kuiper[b], Max Baeten[b], and Daren Dillon[a]

[a]University of California Santa Cruz, 1156 High St, Santa Cruz CA, USA;
[b]TNO Technical Sciences, Delft, The Netherlands

ABSTRACT

Advancements in high-efficiency hybrid-variable reluctance actuators are an enabling technology for building the next generation of large-format deformable mirrors, including adaptive secondary mirrors. In this paper, we evaluate the dynamic performance of two deformable mirror technologies constructed by The Netherlands Organization for Applied Research (TNO) in the context of future use in extreme adaptive optics systems: the 19-actuator FLASH deformable mirror and the DM16 axially symmetric 16mm-pitch actuator. We achieved high-speed measurements (1kHz) utilizing both capacitive sensors and the Quadrature Polarization Interferometer located at the UC Santa Cruz Laboratory for Adaptive Optics.

Keywords: Large-format deformable mirrors, Adaptive secondary mirrors, Hybrid variable reluctance actuators, High-contrast imaging

1. INTRODUCTION

The Netherlands Organization for Applied Research (TNO) has made significant breakthroughs in large-format deformable mirror technology that could enable the next generation of adaptive secondary mirrors to become simpler and less costly to operate. The key advancement is a new style of hybrid variable reluctance (HVR) actuator that is ∼75 times more efficient than traditional voice-coil actuators (HVR actuator efficiency [3] $= 38N/\sqrt{W}$; MMT and LBT actuator efficiency [5] $= 0.5N/\sqrt{W}$). The low required power offers a pathway to eliminate the actuator cooling system, miniaturize the system, and pack the actuators at higher density. TNO is also developing solutions, in conjunction with partners and the Fraunhofer Institute and the University of California Santa Cruz, that could simplify the facesheet fabrication process through hot-forming thin, commercially-available glass sheets.

While the TNO large-format mirrors show great potential to make advanced adaptive optics systems accessible to a wide variety of observatories, they have yet to be proven to the astronomical community. This paper presents the performance testing of TNO's fourth deformable-mirror prototype, the First Lab for adaptive optics Adaptive

Further author information: (Send correspondence to RBR)
E-mail: rbowru@ucsc.edu

Secondary Holophote (FLASH) and the initial performance results from TNO's latest actuator design with 16mm pitch (DM16 actuator). We focus on the dynamic performance of the technology at speeds relevant to extreme adaptive optics system performance ($>$ 1kHz).

Unexpected transient behaviors at speeds greater than $>$ 1kHz have been found in other types of deformable mirrors which could limit our performance when operating at extreme AO speeds if not accounted for carefully. For example, Strobele et al. 2022 [7] used a highspeed camera coupled with a Shack-Hartmann wavefront sensor to evaluate the transient phenomenon in the ALPAO DM 97-15 at speeds up to 16 kHz. They identified a ringing behavior in the mirror's facesheet at frequencies over 1.2 kHz when the actuator move was completed in a single step. In this paper, we aim to study such behavior for the TNO large-format deformable mirror technology.

This is the third in a series of papers documenting the behavior of the TNO large format deformable mirrors. This paper builds upon Bowens-Rubin et al. 2020 [2] and Bowens-Rubin et al. 2021 [1] which reported the initial results of linearity, hysteresis, actuator cross-coupling, measured actuator spacing, drift, lifetime testing for the DM3 and FLASH deformable mirrors.

2. TECHNOLOGY OVERVIEW

2.1 19-actuator FLASH Prototype

The specifications of the FLASH design, its actuators, and the facesheet fabrications and are discussed in detail in Bowens-Rubin et al. 2021 [1] and briefly summarized in Table 1.

The HVR actuators (yellow, right photo in Figure 1) are plugged into a breadboard located on the back of the mirror assembly (blue, right photo in Figure 1). The control electronics are external to the deformable mirror and are connected to the actuator breadboard by ethernet cables. Each ethernet cable controls the signal to four actuators. The electronics can produce an applied voltage of up to +10V across each actuator.

FLASH is controlled through a 64 analog output from a Real Time Linux environment. The user can control the shape of the mirror's surface by specifying the value of the current applied to each of the 19 actuators in an RDA interface in MATLAB running on an office PC. A lead filter was built into the MATLAB control software to speed up the actuator movements from displaying overdamped behavior to being critically damped (tuning parameters: $A = 0.6$, $B = 2.18$, $C = -1.478$, $D = 9.058$).

The roll-off frequency in FLASH was previously measured to be at 40 Hz [1]. Mechanical resonances have previously been demonstrated to show in FLASH at frequencies above $>$ 1.2 kHz [1].

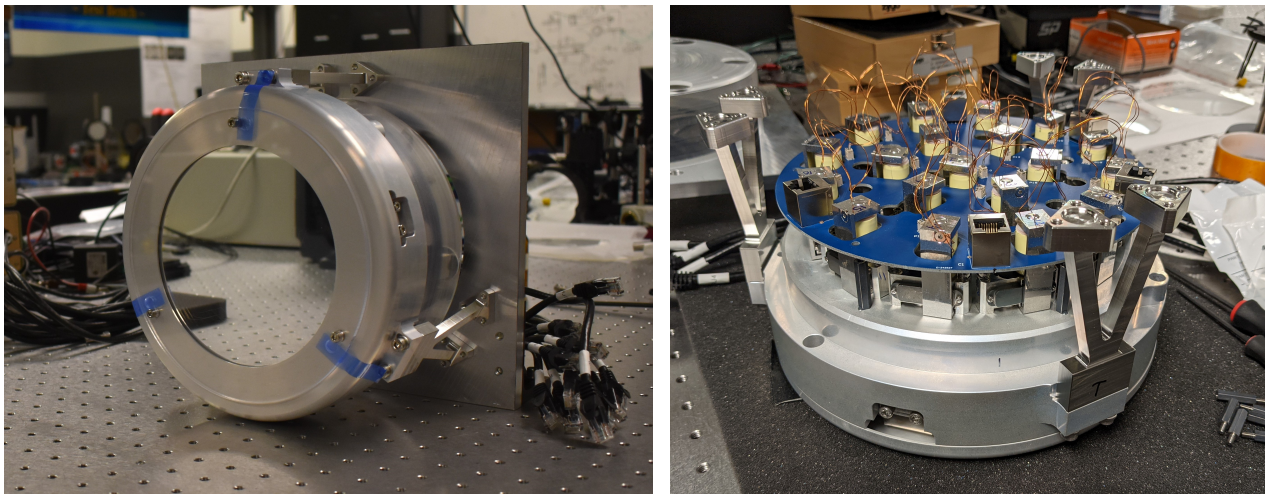

Figure 1. **FLASH 19-Actuator Large-Format Deformable Mirror**. (*Left*) The FLASH mounted on the testbench at the UC Santa Cruz Lab for Adaptive Optics. It is pictured here with its protective mirror-facesheet cover on. (*Right*) Back side of the FLASH mirror with the actuators and electronics breadboard. The ethernet cables and external control electronics are not pictured here.

Table 1. **FLASH Specifications**

Total Diameter	160mm
Facesheet Diameter	150mm
Number of Actuators	19
Actuator Spacing	39mm
Actuator Generation (year)	2020
Actuator Layout Geometry	Hexapolar
Facesheet Thickness	3.3mm
Facesheet Material	Borofloat
Control Electronics Used for Testing	Analog
Available Capacitive Sensor Locations	13

2.2 DM16 Actuator & Testing Jig

The DM16 actuator design from TNO has a 16mm pitch and was completed in 2022. Unlike the design of the previous hybrid-varible reluctance actuators from TNO, the DM16 is axial symmetric. The axial symmetry improves the compact design of the actuators allowing for improved actuator density in future adaptive secondary mirrors.

The inductance of the DM16 actuator was measured to be 14.7±0.05mH, and the resistance was measured to be 2.7±0.05Ω. The maximum operating range of the DM16 actuator was 62μm. Our testing operated within a range of approximately 30μm.

Testing of the DM16 actuator consisted of a single actuator mounted with a capacitive sensor in an aluminium testing jig (pictured in Figure 2). The actuator was screwed into a mounting block on the jig, and the end of the actuator rod connected to a metal strut to provide resistance as if it were attached to a glass facesheet in a deformable mirror. The actuator was driven by an analog input with typical ranges of ±300 mA. Measurements of the settling time and hysteresis were conducted utilizing the TNO provided current driver and MATLAB software, allowing for a specific desired current to be applied to the actuator.

Measurements of the linearity were conducted by manually applying voltages with a power supply. A resistor of 15Ω was placed in series with the actuator in order to allow for current across the actuator to be measured using the applied voltage across the entire circuit.

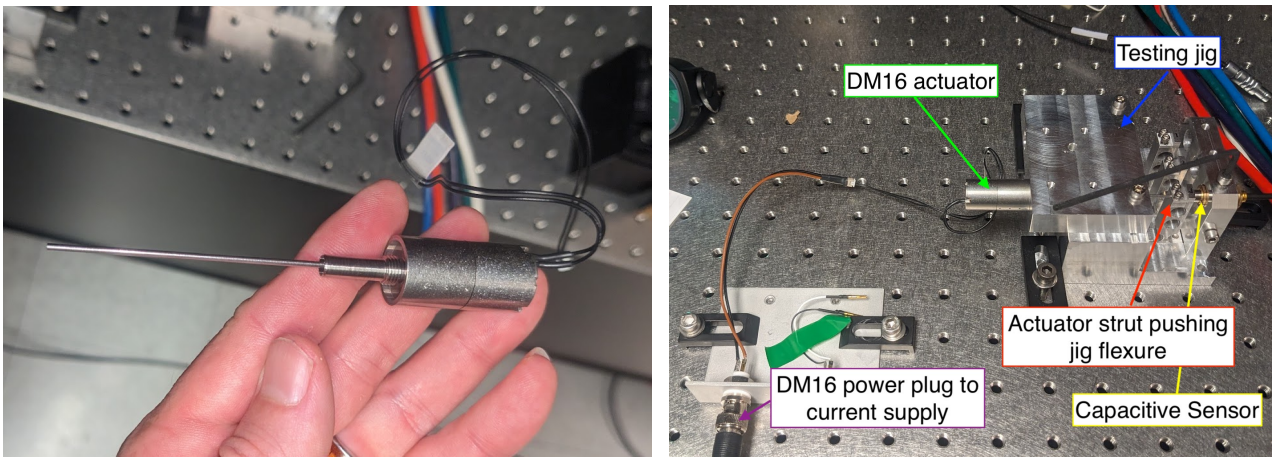

Figure 2. **DM16 Actuator Testing Jig**. (*Left*) The rotationally symmetric DM16 actuator designed by TNO. (*Right*) The testing jig with capacitive sensor used to test the DM16 at the UCSC Lab for Adaptive Optics.

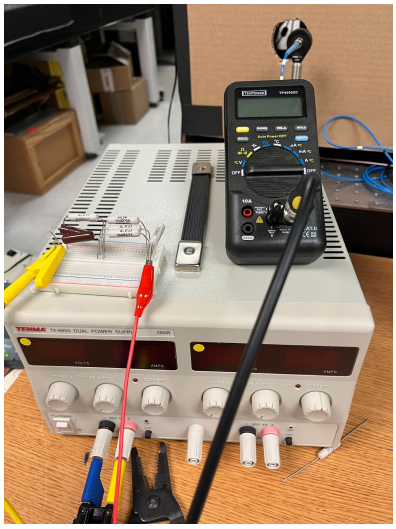

Figure 3. **DM16 actuator electronics setup for linearity testing**. A resistor line was placed in series with the actuator. We used a multi-meter to measure the voltage and resistance across the entire circuit from the power supply output to ground.

2.3 Capacitive Sensor Measurement Setup

FLASH is the first large-format deformable mirror from TNO to incorporate space for an internal capacitive sensor system. The capacitive sensor system can provide data with a readout speed of 3906Hz over a working range of 50μm. However, the capacitive sensor data are limited spatially, capturing displacement information at one point per integrated sensor. The FLASH backing structure has thirteen holes available for capacitive sensors to be mounted. Four Micro Epsilon CS005 capacitive sensors were internally mounted for testing the FLASH at the UCSC-LAO (Figure 4, *left*). The sensors were run using the Micro-epsilon capaNCDT 6200 controller and the Micro-epsilon web interface software in an open loop system.

The mounts to position the capacitive sensors directly behind the mirror facesheet were designed by UC Santa Cruz. They were manufactured out of aluminum and are are 60mm in length. The capacitive sensor is glued in place on the mounting tube (Figure 4, *right*). To install the capacitive sensor mounts in the FLASH backing structure, the actuators were unplugged from the actuator electronics breadboard, and the breadboard was removed and reinstalled.

2.4 Quadrature Polarization Interferometer Testbench

The layout of the Quadrature Polarization Interferometer (QPI) at the UCSC Lab for Adaptive Optics is shown in Figure 5 and described in detail in Laguna et al. 2023 [4]. QPI is a Mach-Zehnder interferometer which can be used to measure the phase of an optic to the spatial resolution of the detector. A HeNe laser source is polarized by a linear polarizer which converts the laser polarization from linear to circular. The light is then split by 4-inch beam splitter cube to create a test and reference path (traced in red and blue respectively in Figure 5). The field of view on the test path is expanded using a one-to-four-inch Zygo beam expander in order to measure a four inch circular patch of the TNO FLASH mirror. The light on the test path is then polarized using a half waveplate. The light on the reference path is reflected off a reference mirror and then polarized using a quarter waveplate. This creates a 90° phase offset between the two paths. The light from the paths is combined and then split using a polarized beam splitter to two Thorlabs HT-5000-S Emergent Cameras.

The software for the Thorlabs cameras was modified in-house to allow for subframing to increase the readout speed. Table 2 gives a summary of the readout speed achievable as a function of subframe size. The max subframe speed available for the camera in the 16x16 subframing mode was 2800 Hz. The size of 128x128 provided the smallest area which could more practically be used for spatial imaging and was usable at 1 kHz speeds.

Although QPI was mounted on a floating optical bench, we found that the stability of the measurements were dependant on the lab acoustics. A cardboard screen was constructed around QPI to minimize the disturbance

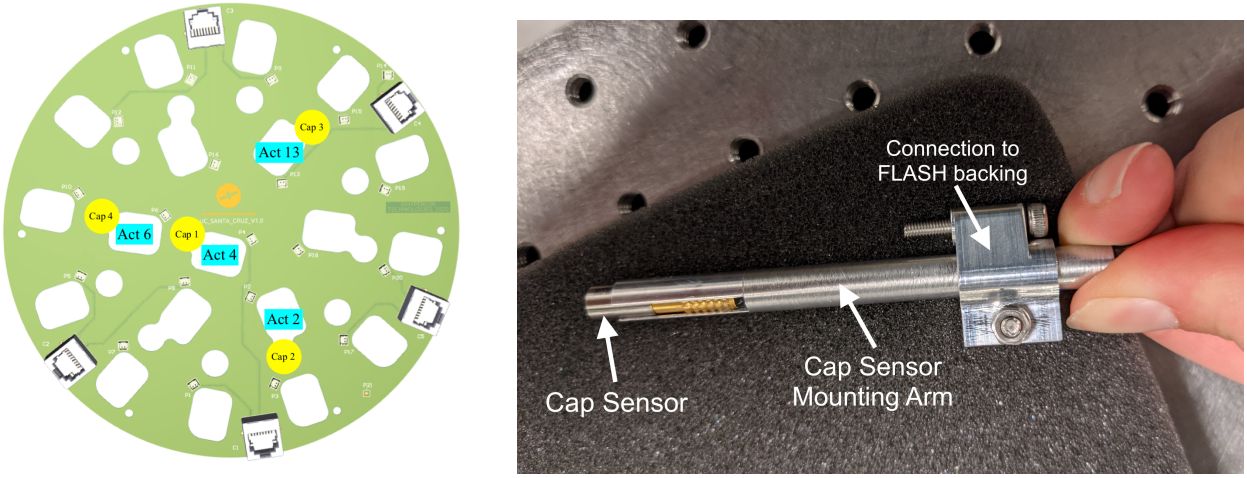

Figure 4. **FLASH Capacitive Sensors**. (*Left*) Four capacitive sensors were added to the internal structure of FLASH for testing at UCSC-LAO. (*Right*) A capacitive sensor inside its mount before it was installed in the back of FLASH.

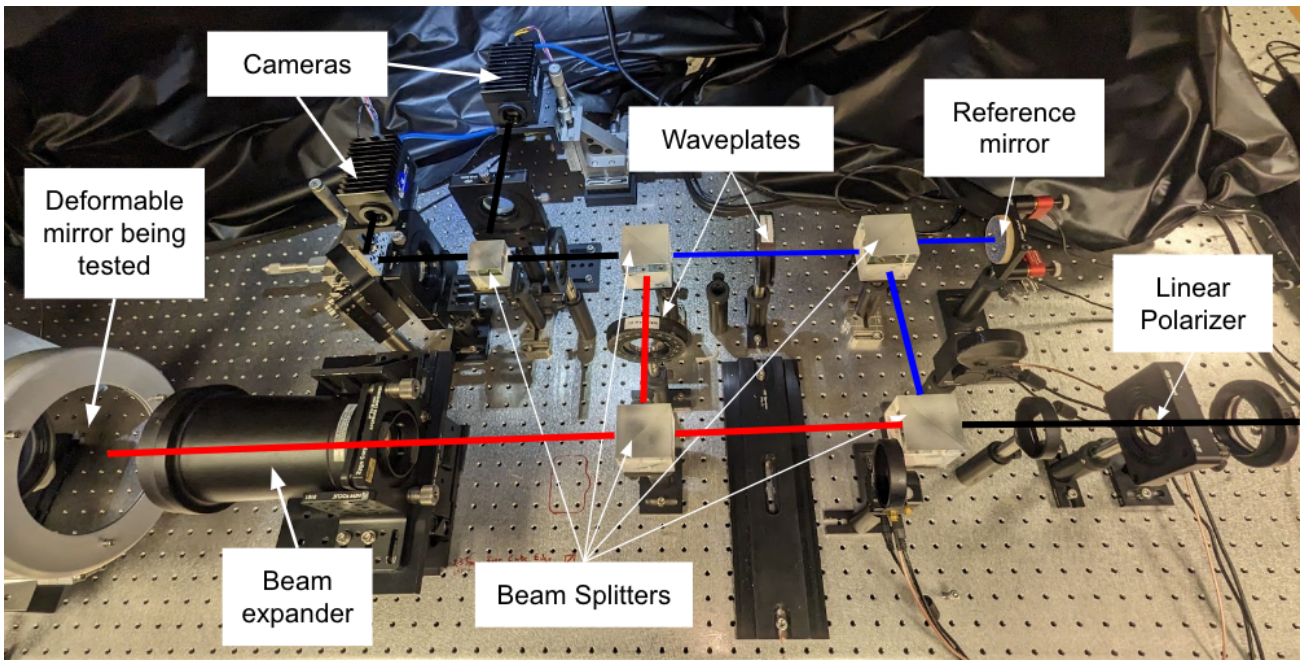

Figure 5. **Quadrature polarization interferometer (QPI)**. The QPI testbench is located in the UC Santa Cruz Lab for Adaptive Optics on a vibration isolated floating optical table. The test arm beam path is traced in red and the reference path is traced in blue. FLASH was placed in the test arm beam path to measure its dynamic behavior spatially.

from sound and air flow. After the overhead filtering fans for the lab's clean room system were were powered down to reduce the noise, the loudest sources of noise near QPI were the fans from the electronics and computers that were needed to power and control FLASH. The sound spectral analysis of the lab at the time that testing was conducted is shown in Figure 6. The loudest tone was near 300 Hz.

3. RESULTS

3.1 DM16 Actuator Settling Time

To quantify the response time for an actuator to reach its final position after a current step is applied, we used the capacitive sensor in the test jig to measure the settling time of the DM16 actuator. Our definition of settling

Table 2. **QPI Camera Readout Speed**

Subframe Size	Camera Max Readout Speed
2048	30 Hz
1024	100 Hz
128	1000 Hz
64	1200 Hz
16	2800 Hz

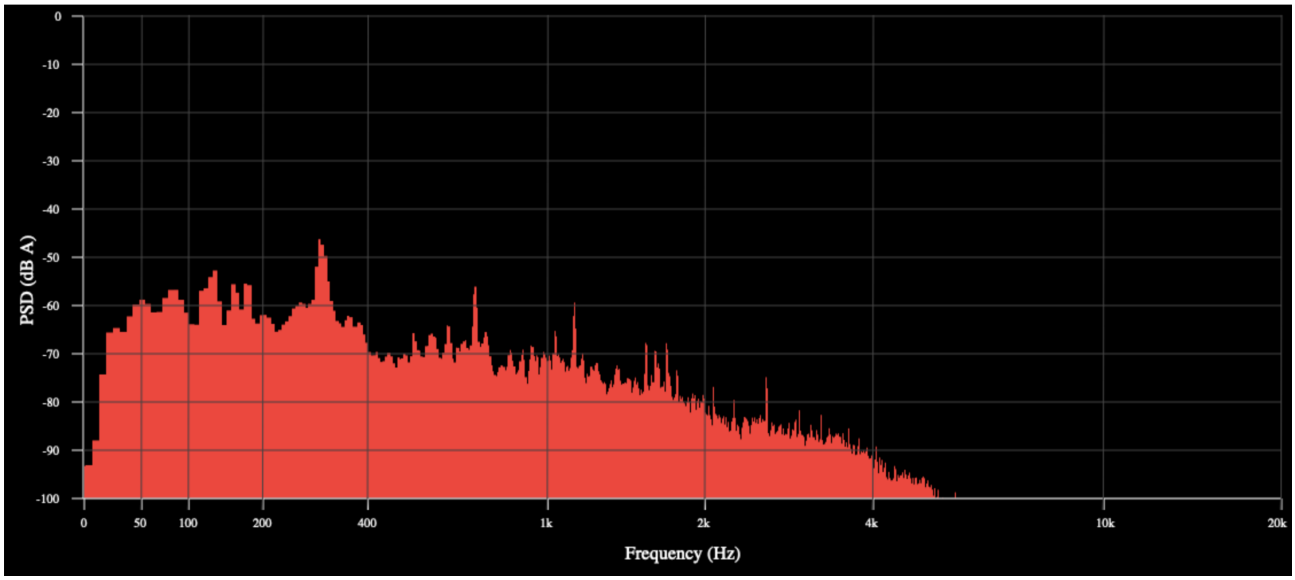

Figure 6. **Sound profile of the Lab for Adaptive Optics near the QPI test bench.** This plot was made using the Spectral Analysis tool on checkhearing.org. The sound profile was recorded approximately five minutes before testing was conducted.

time was adopted from Rochette et al. 2018 [6]. The start of the move is defined as the acutator moving 5% of the total displacement from the initial starting position. Completion of the move is defined as the actuator reaching within 5% of the final displacement.

For the settling time tests, the actuator was controlled via the TNO MATLAB current driver, alternating between 0mA and 16mA to create a 1 micron jump. No lead filters or other special control filters were applied. Figure 7 shows the result of the five settling time trials. Taking the average of these trials, the 1μm jump settling time of the DM16 actuators is 1.4±0.4 ms. Ringing behavior appears consistently in the trials, implying that the DM16 actuator is underdamped. This is not consistent with the FLASH actuators which appear to be overdamped in the settling time trials.

3.2 DM16 Actuator Linearity

The linearity of the DM16 actuators was measured by manually applying voltages that were then converted into the corresponding amperage and compared against a least squares linear fit. The range of applied currents was ±350mA. The actuator, with a resistance of 2.7Ω, was connected inline with a series of resistors totaling around 15Ω. This served the purpose of increasing the resistance of the circuit to 2 digits in order to provide an extra digit of precision when measuring resistance as the multi-meter can only measure to one decimal of accuracy. (Figure 8, *left*) shows the setup used to test linearity. Between each measured displacement the actuator was reset to 0mA by disconnecting and reconnecting the circuit. This avoided additional error caused by hysteresis.

The linearity was calculated by finding the average percentage deviation from the ideal least squares regression line. The maximum deviation was taken as the greatest absolute deviation from the least squares regression.

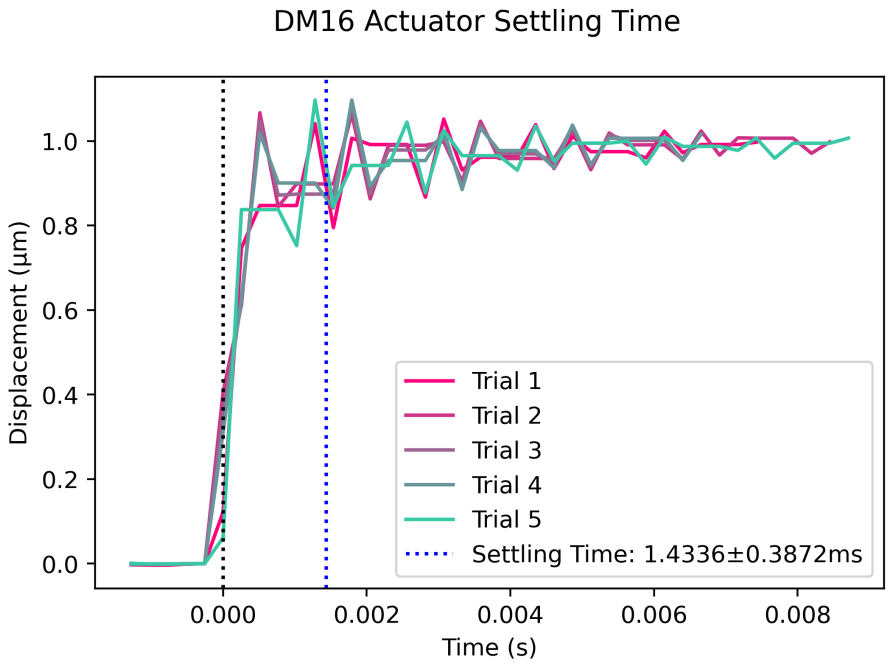

Figure 7. **DM16 Settling Time**. Five trials were averaged to find the DM16 settling time ($t_{set} = 1.4 \pm 0.4$ms).

Linearity of the DM16 actuator was found to be 98.07±0.022% with a maximum deviation of 7.13% (Figure 8, *center, left*).

If the linearity is fit using the full data set from ±300mA, we find that the max deviation is significant (> 6% at the edge cases) with a slope of 48.7 nm/mA (Figure 8). However, the linearity of the actuator is significantly improved if the data fit is split at −100 mA (linearity residual < 1%) (Figure 9). In this "broken" fit, values under −100 mA have a linearity of 99.97 ±0.20% and a maximum deviation of 0.055%. Values over -100mA have a linearity of 99.49 ± 0.17% with a maximum deviation of 0.94%. These two fits have a slope of 40.6 nm/mA (from −300 mA to −100 mA) and 52.0 nm/mA (from −100 mA to 300 mA).

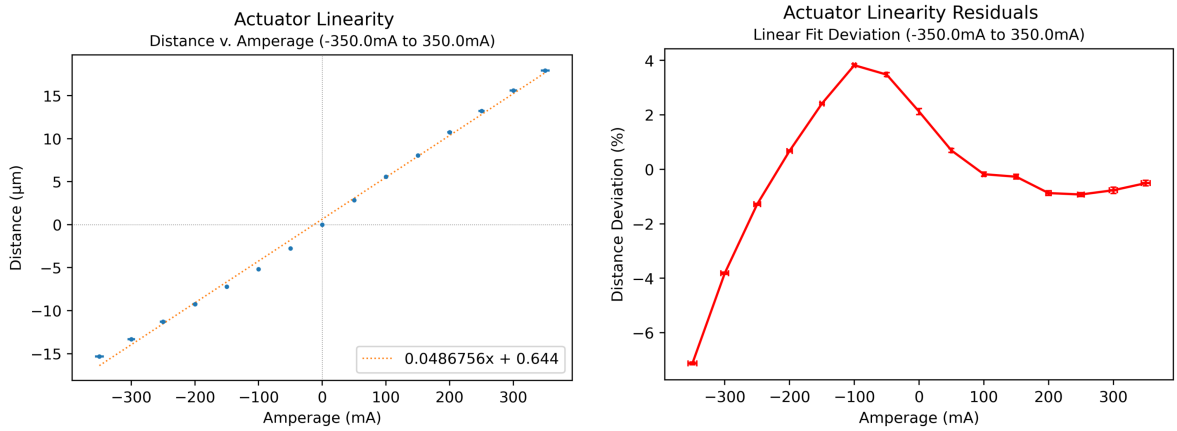

Figure 8. **DM16 Linearity Setup**. (*Left*) The displacement measured by the capacitive sensor (blue) was fit with a linear equation (red) to find quantify the linearity. We measured a slope of 48.7 nm/mA. (*Right*) The residuals from the linear model are plotted in units of percentage deviation.

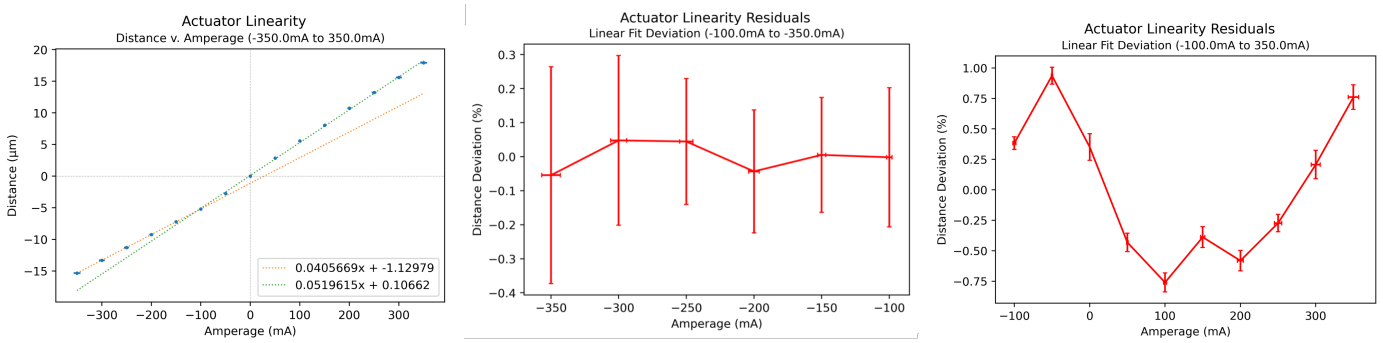

Figure 9. **DM16 Linearity Broken Fit**. (*Left*) DM16 displacement vs amperage with separate least squares regression line for under -100mA and over -100mA. (*Center*) Percentage deviation from linear ideal for DM16 Actuator displacement vs amperage under -100mA. (*Right*) Percentage deviation from linear ideal for DM16 Actuator displacement vs amperage over -100mA.

3.3 DM16 Actuator Hysteresis

Actuator displacement varies depending on the previous position of the actuator. To quantify this effect, the hysteresis of the DM16 actuator was measured using the TNO current drivers. We applied the current pattern stepping up from 0mA to 300mA, then stepping down from 300mA to -300mA, and then back to 0mA.

The average hysteresis of the DM16 actuator is $0.211 \pm 0.001 \mu$m ($0.651 \pm 0.003\%$) with a maximum of 0.302 ± 0.012 μm ($0.93 \pm 0.04\%$). The average hysteresis was calculated by averaging the absolute difference between the upscale and downscale displacement at each amperage. We quantified the percent hysteresis using the definition:

$$Hyst(\%) = 100 \left(\frac{|S3 - S1|}{|S2 - S4|} \right) \tag{1}$$

where $S1$ and $S3$ are the displacements measured at an applied current of zero and $S2$ and $S4$ are the displacements measured at the maximum and minimum current applied.

This measured DM16 average hysteresis value ($0.651 \pm 0.003\%$) is smaller than the hysteresis value measured for the older generation of actuators in FLASH ($1.93 \pm 0.04\%$) [1]. However, we note that the FLASH average hysteresis value was calculated using loops with smaller max/min currents (± 20 - ± 120 mA rather than ± 300 mA).

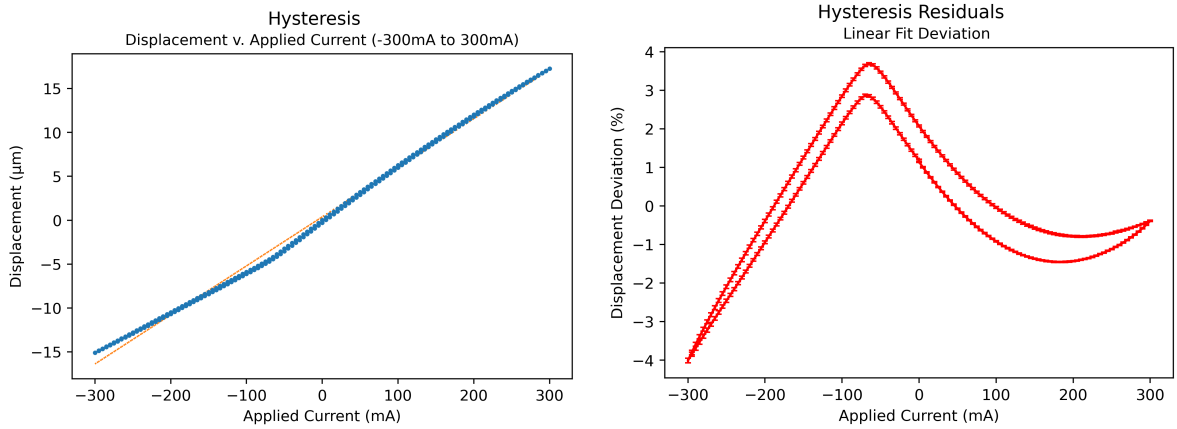

Figure 10. **DM16 Hysteresis Residuals**. (*Left*) The displacement during the hysteresis test with applied currents from ± 300mA (blue) was fit with a single-line linear fit (red). (*Right*) The hysteresis residuals. The deviations shown here (red) were calculated by finding the difference from the linear best fit.

3.4 FLASH Actuator Settling Time

The initial settling time measurements with the FLASH actuators were reported in Bowens-Rubin et al. 2021 [1]. The settling time that was measured with a well-tuned lead filter applied was $t_{set} = 1.08 \pm 0.08$ms for a step of 10mA ($\sim 3\mu m$).

We report the dynamical responses using a set of all-actuator pokes (Figure 11, top) and single-actuator pokes (Figure 11, bottom) at the following applied current values: 1mA, 2mA, 3mA, 4mA, 5mA, 10mA, 15mA, and 20mA. The measurements were collected with the capacitive sensor system internal to FLASH. The center actuator (actuator 4) was used to perform the single-actuator poke. The capacitive sensors make a good approximation for the displacement in the all-actuator poke but not in the single actuator poke because the captive sensor is located approximately half of an actuator spacing from the center of the actuator.

One trial was performed per displacement step. The displacement measurments of these trials are shown side-by-side in Figure 11. We adopted the same $\pm 5\%$ definition from the start/end of the test as we did with the DM16 settling time test to define the duration of the settling time. Our settling time measurements for each trial are plotted in Figure 12.

Our trials were performed with the optimally tuned lead filter from the tuning presented in Bowens-Rubin et al. 2021 [1]. However, we find that this tuning only holds for single-actuator movements with small current steps (≤ 5 mA). Curiously, the tuning did not hold for a step size of 10mA where it was originally tuned. The average settling time for the adequately tuned steps was $t_{set} = 1.0 \pm 0.2$ ms. The movements for the all-actuators trials and the single-actuator trials with current steps of ≥ 10 mA display overdamped behavior. It is possible that a better tuned lead filter for each step size could lead to the desired critically damped behavior, but uniform tuning that applies to all movements does not appear possible.

3.5 FLASH Spacial Dynamical Response

We measured the surface of FLASH using the QPI testbench (described in Section 1) to evaluate the transient behaviors present after moving an actuator. Testing was completed using the center actuator with applied currents of ± 5 mA (± 233 nm displacement). The optimally tuned lead-filter was applied to make this testing consistent with the settling time test.

Measurements were performed using the images from the two QPI cameras with subframe sizes of 1024x1024 (speed 100 Hz) and 128x128 (speed 1.0 kHz). Examples of images from Camera 1 at these subframe sizes are shown in Figure 13. We were not able to use smaller subframe sizes because we were not able to resolve the sides of a fringe in the subframes smaller than 128x128. We normalized the raw images to account for differences in brightness between the test and reference beams using calibration flats. Each flat was the average of ten images and was obtained by blocking the opposite beam (i.e. the reference-beam flat was taken with the test beam blocked).

In our setup's natural steady-state before a move command was applied, we measured a small oscillation at 250 ± 50 Hz. It is presumed that this vibration is due to the measurement setup and lab environment because the frequency is near the peak of the sound profile of the lab (see Figure 6).

We used the 128x128 frames with the speed of 1 ms/frame to study the speed of the actuator movement and the resulting oscillations. The majority of the start and end of the actuator move occurred between two frames, corresponding to a time of ~ 1 ms. This is consistent with our settling time measurements.

No induced oscillations were detected from the actuator pokes within the frequencies probed by our testing (slower than 1kHz). This was expected as the FLASH mechanical resonances occur at frequencies > 1.2 kHz. We aim to continue to improve the QPI setup so that faster frequencies can be probed with QPI in future testing.

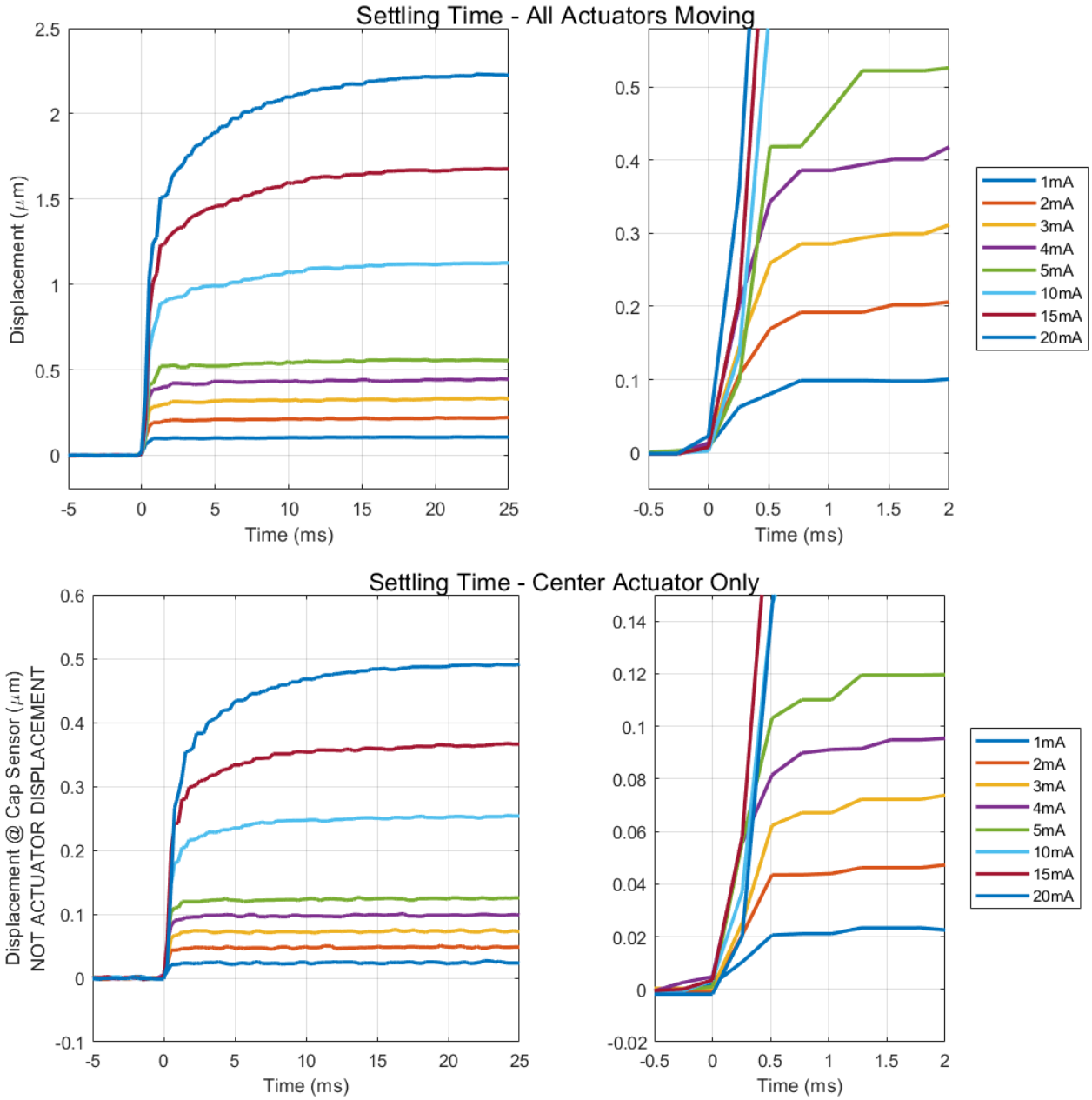

Figure 11. **FLASH Settling Time**. Movements were performed with eight applied currents using two styles of movement: all actuators together and the center actuator only. The testing was performed with the "optimal" lead filter applied, however, we find underdamped behavior in all but the smallest single actuator movements.

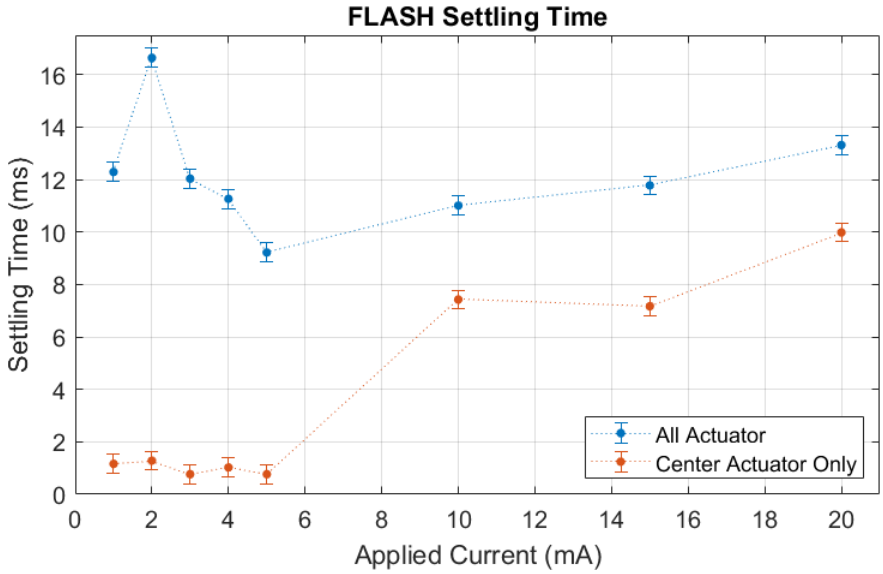

Figure 12. **FLASH Settling Time Measurements**. We measured the settling time using the start/stop time at ±5% the total displacement of the poke. The settling times for the small applied currents ($1 - 5\,\mathrm{mA}$) with the single actuator poke were measured to be < 2ms. The larger measurements of the settling time (> 5ms) correspond to runs displaying overdamped behavior.

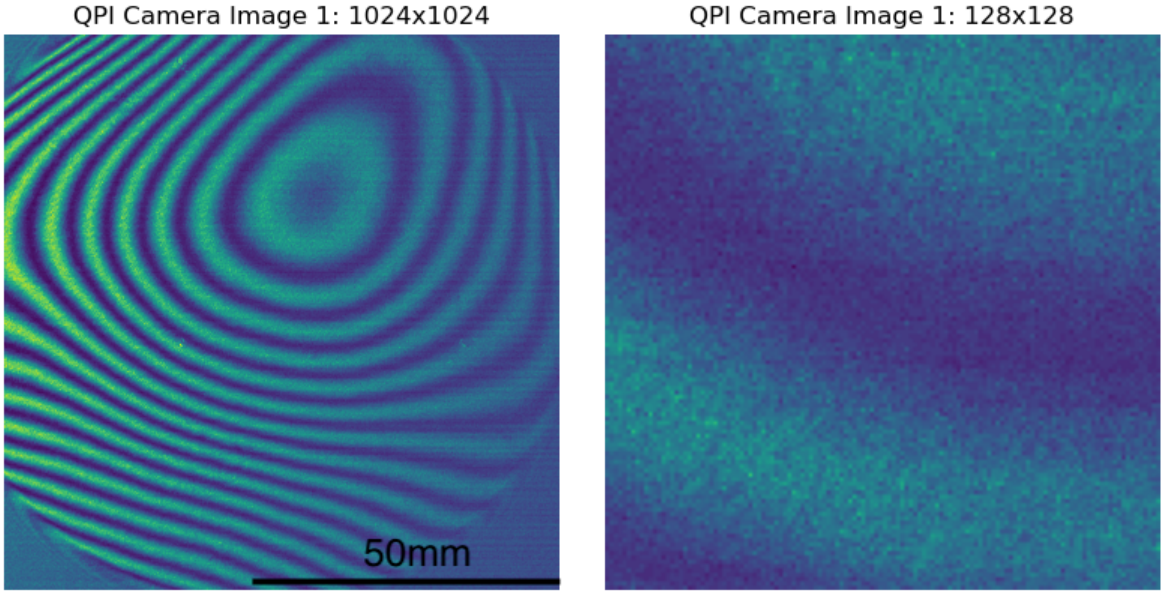

Figure 13. **Images from QPI**. (*Left*) An example image with 1024x1024 subframing. (*Right*) An example image with 128x128 subframing.

4. CONCLUSIONS

The key results from the testing the TNO large-format deformable mirror technology completed by the University of California Lab for Adaptive Optics is summarized in Table 3. We present the initial linearity, hysteresis, and settling time measurements of the rotationally symmetric 16mm-pitch DM16 actuator alongside the settling time and spatial dynamic testing of the FLASH deformable mirror.

We find that the DM16 actuator, like the previous generations of hybrid-variable reluctance actuators from TNO, is strongly linear ($> 99\%$) and has low hysteresis ($< 1\%$). However, unlike previous actuator generations, we find that the DM16 actuator displays two distinct linear regions divided at approximately -100mA. The DM16 settling time test was completed without a lead-filter control and displayed underdamped ringing behavior. The DM16 settling time measurement (1.4 ± 0.4 ms) is consist with the FLASH actuator settling time when the lead-filter was applied to speed up the movement of the FLASH actuators.

Through the FLASH settling time and dynamic measurements, we have identified that the original lead-filter control tuning does not apply universally. We find that no major oscillations were induced by small actuator movements at frequencies < 1 kHz, as expected.

Table 3. **Summary of Testing Results**

Section	Test	Takeaway
3.1	DM16 Actuator Settling Time	$t_{set} = 1.4 \pm 0.4$ ms No lead filter, move of 1 μm (16mA)
3.2	DM16 Actuator Linearity	There are two distinct linear regions with the turning point at -100mA Linearity -300mA - -100mA = 99.97±0.20% Linearity -100mA - 300mA = 99.49±0.17%
3.3	DM16 Actuator Hysteresis	Hyst = $0.651 \pm 0.003\%$
3.4	FLASH Settling Time	Movements without a well tuned lead-filter applied display overdamped behavior. Average for a single actuator movement with a well-tuned lead filter: $t_{set} = 1.0 \pm 0.2$ ms
3.5	FLASH Spatial Dynamics	No oscillations induced by an actuator poke of $\sim 230nm$ were detected at frequencies below 1kHz.

ACKNOWLEDGMENTS

The authors would like to thank Mark Chun, Ruihan Zhang, Sylvain Cetre, Wouter Jonker, Matthew Maniscalco, Joost Peters, and the members of the Lab for Adaptive Optics at UC Santa Cruz for their guidance and assistance in the completion of this work.

References

[1] Rachel Bowens-Rubin et al. "Performance of large-format deformable mirrors constructed with hybrid variable reluctance actuators II: initial lab results from FLASH". In: *Techniques and Instrumentation for Detection of Exoplanets X*. Ed. by Stuart B. Shaklan and Garreth J. Ruane. Vol. 11823. Society of Photo-Optical Instrumentation Engineers (SPIE) Conference Series. Sept. 2021, 118231R, 118231R. DOI: 10.1117/12.2593535. arXiv: 2110.01693 [astro-ph.IM].

[2] Rachel Bowens-Rubin et al. "Performance of large-format deformable mirrors constructed with TNO variable reluctance actuators". In: *Adaptive Optics Systems VII*. Ed. by Laura Schreiber, Dirk Schmidt, and Elise Vernet. Vol. 11448. Society of Photo-Optical Instrumentation Engineers (SPIE) Conference Series. Dec. 2020, 114485V, p. 114485V. DOI: 10.1117/12.2563659. arXiv: 2012.07222 [astro-ph.IM].

[3] Stefan Kuiper et al. "Advances of TNO's electromagnetic deformable mirror development". In: *Advances in Optical and Mechanical Technologies for Telescopes and Instrumentation III*. Ed. by Ramón Navarro and Roland Geyl. Vol. 10706. Society of Photo-Optical Instrumentation Engineers (SPIE) Conference Series. July 2018, 1070619, p. 1070619. DOI: 10.1117/12.2311981.

[4] Cesar Laguna. "Analyzing Variation in Phase Delays Across Phase Plates With a Quadrature Polarization Interferometer". In: *arXiv e-prints*, arXiv:2310.07737 (Oct. 2023), arXiv:2310.07737. arXiv: 2310.07737 [astro-ph.IM].

[5] Armando Riccardi et al. "Adaptive secondary mirrors for the Large binocular telescope". In: *Astronomical Adaptive Optics Systems and Applications*. Ed. by Robert K. Tyson and Michael Lloyd-Hart. Vol. 5169. Society of Photo-Optical Instrumentation Engineers (SPIE) Conference Series. Dec. 2003, pp. 159–168. DOI: 10.1117/12.511374.

[6] Maxime Rochette et al. "Dynamic response of ferrofluidic deformable mirrors using elastomer membrane and overdrive techniques". In: *International Journal of Optomechatronics* 12.1 (Jan. 2018), pp. 20–30. DOI: 10.1080/15599612.2018.1465147. arXiv: 1810.09987 [physics.app-ph].

[7] S. Ströbele et al. "ESO's ultra-fast wavefront sensor unveils the mysteries of deformable mirrors' temporal behaviour". In: *Adaptive Optics Systems VIII*. Ed. by Laura Schreiber, Dirk Schmidt, and Elise Vernet. Vol. 12185. Society of Photo-Optical Instrumentation Engineers (SPIE) Conference Series. Aug. 2022, 1218526, p. 1218526. DOI: 10.1117/12.2627917.